Soft Matter

COMMUNICATION

View Article Online
View Journal | View Issue

Cite this: *Soft Matter*, 2023, **19**, 7691

Received 9th June 2023,
Accepted 30th September 2023

DOI: 10.1039/d3sm00758h

rsc.li/soft-matter-journal

Anisotropic material depletion in epitaxial polymer crystallization†

Jason X. Liu,‡[ab] Yang Xia,‡[a] Yucheng Wang,[c] Mikko P. Haataja,[ab] Craig B. Arnold[ab] and Rodney D. Priestley *[bc]

The physical properties of a semicrystalline polymer thin film are intimately related to the morphology of its crystalline domains. While the mechanisms underlying crystallization of flat-on oriented polymer crystals are well known, similar mechanisms remain elusive for edge-on oriented thin films due to the propensity of substantially thin films to adopt flat-on orientations. Here, we employ an epitaxial polymer–substrate relationship to enforce edge-on crystallization in thin films. Using matrix-assisted pulsed laser evaporation (MAPLE), we deposit films in which crystal nucleation is spatially separated from subsequent epitaxial crystallization. These experiments, together with phase-field simulations, demonstrate a highly anisotropic and localized material depletion during edge-on crystallization. These results provide deeper insight into the physics of polymer crystallization under confinement and introduce a processing motif in the crystallization of ultrathin structured films.

Crystallization of a bulk polymer melt involves the formation of three-dimensional spherulitic structures.[1] However, when confined to films of thickness approaching the lamellar width, polymer crystallites lose orientational freedom and are constrained to adopt flat-on or edge-on orientations in which the chain axis is perpendicular or parallel to the substrate plane, respectively.[2,3] During the growth of flat-on lamellae, a competition between diffusive mass transport and crystallization yields a variety of morphologies ranging from dendritic to seaweed-like to faceted crystals.[4] On the other hand, edge-on oriented crystallites are constrained to grow in needle-like structures since crystal growth only occurs along the crystalline facets and not on the amorphous fold surfaces.[5,6]

The mass transport processes which lead to structure formation in flat-on crystallites are well-explored, however, such mechanisms remain elusive for edge-on oriented thin films. While several works have followed the growth kinetics of individual edge-on needles, these were grown in several hundred nanometer thick films in which two-dimensional spherulites formed.[6–9] In this communication, we elucidate the mechanisms of edge-on polymer crystal growth in thin films. We utilize an epitaxial polymer–substrate relationship to enforce edge-on crystallization in films which would otherwise adopt the flat-on orientation.[10–12] Our experiments, together with phase-field simulations, reveal that amorphous material depletion during edge-on epitaxial crystallization is highly anisotropic, in contrast to material depletion for flat-on crystal growth. We additionally demonstrate that epitaxial alignment is gradually lost as polymer crystallization occurs at higher crystallization temperatures. These results provide greater insight into the physics of polymer crystallization under confinement and epitaxy and additionally introduce a new processing motif in the crystallization of oriented epitaxial crystals.

To obtain epitaxial polymer thin films, we employ matrix-assisted pulsed laser evaporation (MAPLE) to deposit poly(ethylene oxide) (PEO, $M_w = 12 \times 10^3$ g mol^{-1}) atop freshly cleaved muscovite mica substrates (epitaxial relationship in Fig. S2, ESI†). In MAPLE, a pulsed laser is used to ablate a frozen, dilute polymer solution target under vacuum,[13] and film growth subsequently proceeds *via* an accumulation of polymer droplets ranging in size from tens of nanometers to several microns.[14] Previous work has demonstrated that when employing MAPLE to deposit semicrystalline polymers, smaller deposited droplets are unable to undergo primary crystal nucleation and instead flow to cover the substrate, forming an amorphous liquid layer.[15] Nucleation occurs only when a polymer droplet of sufficient size is deposited, due to the reduced ability of a crystal to nucleate when confined to dimensions approaching or below the size of a critical

[a] *Department of Mechanical and Aerospace Engineering, Princeton University, Princeton, NJ 08544, USA*
[b] *Princeton Materials Institute, Princeton University, Princeton, NJ 08544, USA. E-mail: rpriestl@princeton.edu*
[c] *Department of Chemical and Biological Engineering, Princeton University, Princeton, NJ 08544, USA*

† Electronic supplementary information (ESI) available. See DOI: https://doi.org/10.1039/d3sm00758h

‡ These authors contributed equally.

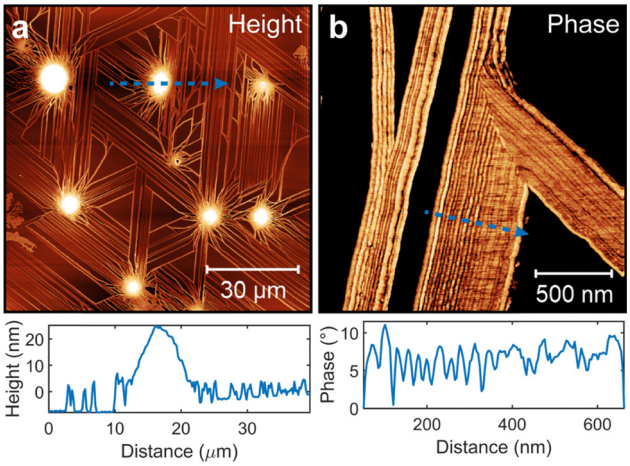

Fig. 1 Atomic force microscopy images of the hierarchical morphology of MAPLE-deposited epitaxial films of polyethylene oxide atop muscovite mica. Height and phase profiles are extracted along the blue dotted lines. (a) Height image showing a large-scale view containing a collection of isolated droplets surrounded by a film of epitaxially aligned needles. (b) Phase image showing the structure of a junction between two differently oriented epitaxial needles. Individual lamellae comprising the needle are readily visible.

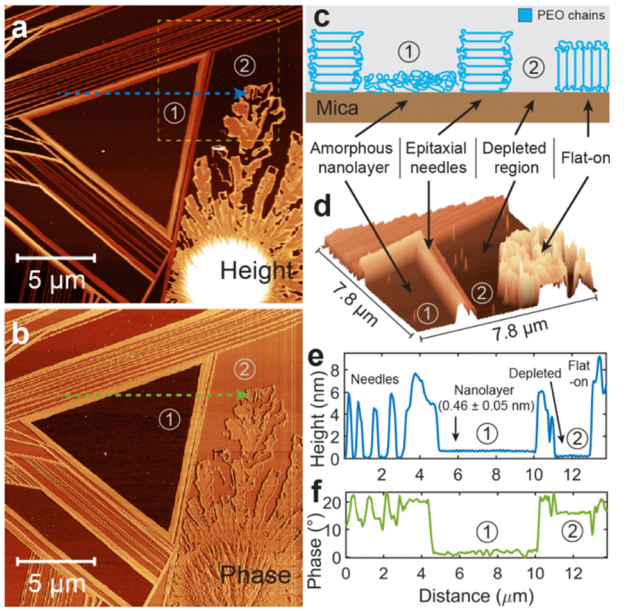

Fig. 2 Formation of a residual amorphous nanolayer due to the highly anisotropic crystallization of epitaxial needles. (a) AFM height image of a region of the substrate enclosed by epitaxial needles forming an equilateral triangle. (b) AFM phase-contrast image of the same region. (c) Schematic depicting edge-on needles acting as a barrier to amorphous chain diffusion (not to scale). The amorphous nanolayer is depleted in the region containing flat-on polymer crystals. (d) Three-dimensional height view of the region in panel (a) enclosed by the dotted yellow square. (e) Height profile along the dotted blue line in (a). (f) Phase shift profile along the dotted green line in (b).

nucleus.[16,17] Thus, MAPLE enables us to spatially separate crystal nucleation from subsequent growth, yielding a route to thin film crystallization in which epitaxially aligned edge-on crystals grow outwards from central droplets.

We perform short MAPLE depositions to obtain partially consolidated films (see Experimental Methods in the Supplementary Information). In Fig. 1a, atomic force microscopy (AFM) reveals a hierarchical morphology of epitaxially aligned needles which are observed to radiate outwards from crystalline, spherulitic microdroplets (Fig. S3, ESI†). Due to the epitaxial PEO–mica relationship, the edge-on morphology is primarily observed where otherwise flat-on crystallites would form (Fig. S4, ESI†). The edge-on morphology is apparent Fig. 1b, where polymer lamellae are observed to bundle together, forming several hundred nanometer-wide needles composed of multiple laterally adjacent lamellae, approximately 5–10 nanometers in height (Fig. S5, ESI†).

In our experiments, we find that epitaxial needles form enclosed, geometric shapes such as the equilateral triangle in Fig. 2a and b when growing needles meet or when secondary nucleation occurs along the length of a pre-existing needle and subsequent growth follows the six-fold symmetry of the underlying substrate. Intriguingly, AFM scans reveal the existence of an amorphous nanolayer within the enclosed triangular domain: Fig. 2e depicts a height trace along the blue dotted line of Fig. 2a, where a 0.46 nm height difference can be seen between regions ① and ②. We attribute the presence of this uncrystallized nanolayer to the fact that during crystallization, the amorphous film is only depleted locally, along the path of the growing needle. Thus, when epitaxial growth forms an enclosed domain, the uncrystallized film becomes bounded by the amorphous fold surfaces of the epitaxial needles, as illustrated in Fig. 2c. These bounded, uncrystallized polymers can only be depleted *via* secondary crystal nucleation on the amorphous fold surfaces of the enclosing lamellae, which manifests as the widening and thickening of the bounding needles compared to the externally adjacent ones (see the taller and thicker needles adjacent to the nanolayer in Fig. 2e). However, this process is comparatively slow,[18] so the amorphous layer is not fully depleted prior to characterization.

These crystallization mechanics contrast with those of flat-on crystals. A flat-on oriented polymer lamella can grow in all in-plane directions since a crystalline surface is presented to the amorphous melt film regardless of direction. Thus, any amorphous material which is adjacent a flat-on crystal, such as in region ②, is free to diffuse and join the exposed crystalline surfaces. Polymer chains then become fully depleted in these regions, exposing the underlying mica substrate. The phase-contrast image in Fig. 2b reveals a difference in AFM phase lag of about 14° between regions ① and ②. This further corroborates the existence of an uncrystallized nanolayer since adhesion between the AFM tip and an amorphous polymer film will induce a viscoelastic response during AFM tapping which a bare mica surface will not.[19] This variation in phase contrast also indicates that different bounded domains will have varying extents of material depletion and thus phase lag, as observed in Fig. S6 (ESI†).

To obtain deeper physical insight, we simulate this anisotropic crystallization process with a 2D phase-field model. The

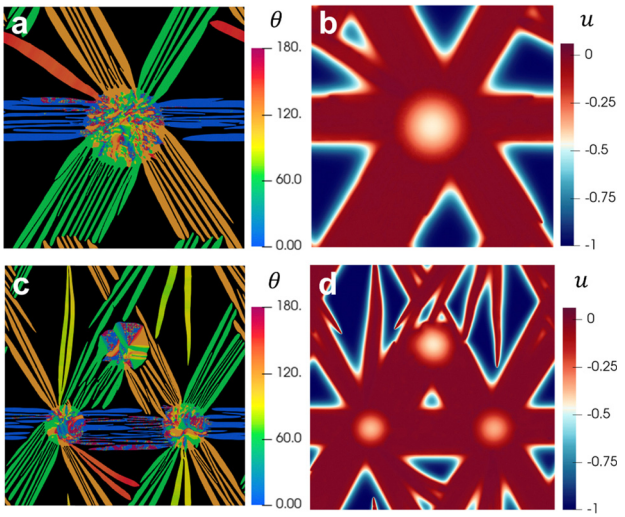

Fig. 3 Phase-field simulations of the epitaxial crystallization of edge-on lamella. (a) Crystal morphology of a single droplet surrounded by epitaxial needles, colored according to the local crystal orientation direction, θ. (b) Map of the dimensionless concentration, u, of remaining amorphous polymer in panel (a). $u = -1$ corresponds to the initial concentration while $u = 0$ corresponds to a fully depleted concentration. (c) Spherulites and epitaxial needles formed by three adjacent droplets and (d) their corresponding amorphous polymer concentration field.

model recapitulates the crystallization of edge-on polymer lamellae by introducing a crystal interfacial energy which induces crystal growth only parallel to the crystal orientation direction, attaining no growth in the orthogonal directions. A six-fold azimuthally symmetric potential energy well models the substrate epitaxial directions, and a densification parameter, Δ, dictates the degree of densification which occurs during the amorphous–crystalline phase transition. For regions in which $\Delta < 1$, only a fraction, Δ, of the system area will be crystalline when the amorphous starting material is fully depleted. Thus, to mimic variations of height in our 2D model, we initialize a circular region with $\Delta = 2$ to represent the central droplet, and at the edge of the droplet, we impose a smooth transition to $\Delta = 0.5$ to model the transition from thick droplet to thin film (see Simulation Methods in the ESI†).

A representative simulation morphology grown from an initial seed crystal in the center of the droplet is shown in Fig. 3a and b. A fully dense crystal structure is observed in the center of Fig. 3a, reflecting the fact that $\Delta > 1$ in this region. In Fig. 3a, the crystalline phase is colored according to the local crystal orientation angle, θ, and azimuthal variations in crystal orientation are observed within the droplet, indicating a spherulitic internal structure (also see Fig. S7, ESI†). When the crystal growth front reaches the thin film region, Δ becomes less than 1, and the area covered by the final crystalline state is less than that covered by the initial amorphous phase.[20] Thus, regions devoid of the crystalline phase necessarily form. Coupled with the highly anisotropic crystallization set by the interfacial energy, this results in the formation of distinct, well-oriented needle-like structures, as observed experimentally.

The concentration field of the amorphous phase is shown in Fig. 3b, and this concentration map reveals that amorphous material is only depleted locally, along the growth trajectory of epitaxial needles. While the dimensionless concentration, u, is fully depleted to $u = 0$ within the bands containing epitaxial needles, the adjacent regions remain at their initial value of $u = -1$. In Fig. 3c and d we show the simulated morphology of three adjacent droplets, all seeded with crystal nuclei. The simulation demonstrates that needle growth is arrested due to material depletion when needles impinge on one another. When a set of blocked needles encloses a domain of uncrystallized material, as in the very center of Fig. 3c and d, then that amorphous material persists due to the low crystal growth rate in directions orthogonal to the crystal orientation. Thus, multiple factors lead to the experimental observations in Fig. 2. Since material depletion occurs only locally along the path of growing epitaxial needles, substantial uncrystallized material persists in the thin film region. When epitaxial needles impinge upon one another, growth is inhibited, and due to the preferred crystallization along epitaxial directions, this leads to amorphous material enclosed within geometric domains.

Finally, to probe the effect of temperature on crystallization morphology, we perform MAPLE depositions at various substrate temperatures ranging from 20–60 °C. The resulting AFM images in Fig. 4 demonstrate that epitaxy is gradually lost with an increase in deposition temperature. Well-aligned needles are initially observed at 20 °C and 35 °C (Fig. 4a and b); however, at 45 °C, the orientational order of edge-on needles is lost, as seen in Fig. 4c. Rather than growing along epitaxial directions, edge-on needles attain curved morphologies as they respond to random fluctuations in the local direction and

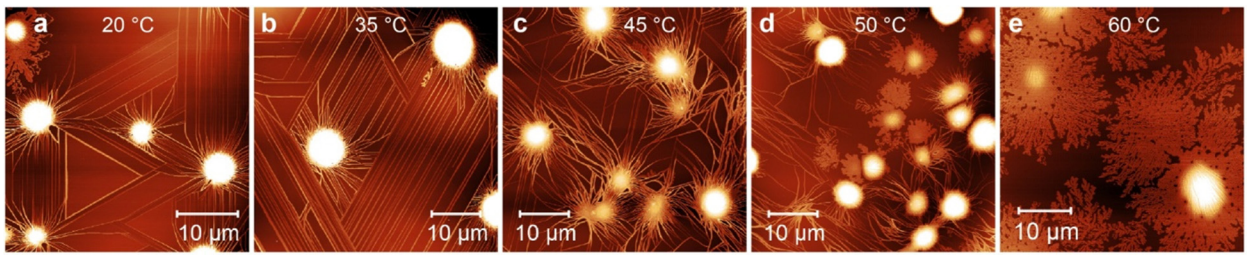

Fig. 4 Temperature dependence of the crystallization morphology. (a)–(e) AFM height images of films deposited at varying substrate temperatures between 20–60 °C, as indicated in the image. Epitaxially oriented edge-on needles are observed at 20 °C and 35 °C, while at 45 °C and 50 °C edge-on needles lose their epitaxial alignment. At 60 °C, only flat-on dendritic crystals are observed.

magnitude of material flux arriving at the needle tip. At the yet higher temperature of 60 °C, edge-on lamellae in Fig. 4e are no longer present, and only flat-on dendrites are observed. At these temperatures, even if the substrate acts as a heterogeneous nucleation site for an incipient edge-on crystal, we hypothesize that subsequent growth within the droplet has little energetic incentive to continue in the edge-on orientation and the growing crystal may rotate into an arbitrary orientation, eventually leading to the flat-on geometry in the thin film region.[12,21] These mechanics differ from those of flat-on films, for which the substrate temperature dictates a competition between diffusion and the driving force for crystallization, thus determining the resulting crystal morphology.[22] These experiments demonstrate that since in edge-on crystallization, needles can only grow in a direction along their crystalline facets, the only morphological transition we observe in edge-on growth is loss of epitaxial alignment upon an increase in substrate temperature.

Future work investigating the kinetics of epitaxial crystallization will provide further insight into processes such as the competition between surface chain mobility and crystallization. Since material depletion is highly localized to the tip of the growing edge-on needle, it is unlikely that a substantial depletion zone forms ahead of the growing crystal front. This implies that crystal growth may be limited by the rate of chain attachment on the crystalline surface, rather than by diffusive mass transport to the growing tip, as is the case for flat-on crystals. Additionally, while here we achieve these morphologies using MAPLE deposition, these results may be extended to other patterned deposition techniques which allow for spatial separation of nucleation from growth, such as inkjet printing. These results provide new insight into polymer epitaxy under confinement and introduce a new motif in the creation of oriented crystals.

Conflicts of interest

There are no conflicts of interest to declare.

Acknowledgements

This work was supported by the National Science Foundation (NSF) Materials Research Science and Engineering Center Program through the Princeton Center for Complex Materials (PCCM) (DMR-2011750). The authors acknowledge the use of Princeton's Imaging and Analysis Center (IAC), which is partially supported by the NSF *via* PCCM. The authors would like to thank Prof. Richard Register, Prof. Robert Prud'homme, Prof. Nan Yao, Dr Guangming Chen, Mr John Schreiber, and Mr Geoffrey Zheng for their insightful discussions. The authors would also like to thank Mr Clark Caplan of PVD Products Inc. for his assistance with the infrared MAPLE system.

References

1 B. Crist and J. M. Schultz, Polymer spherulites: A critical review, *Prog. Polym. Sci.*, 2016, **56**, 1–63.
2 Y. X. Liu and E. Q. Chen, Polymer crystallization of ultrathin films on solid substrates, *Coord. Chem. Rev.*, 2010, **254**(9–10), 1011–1037.
3 G. Reiter and J. U. Sommer, Crystallization of adsorbed polymer monolayers, *Phys. Rev. Lett.*, 1998, **80**(17), 3771–3774.
4 G. Zhang, X. Zhai, Z. Ma, L. Jin, P. Zheng and W. Wang, *et al.*, Morphology diagram of single-layer crystal patterns in supercooled poly(ethylene oxide) ultrathin films: Understanding macromolecular effect of crystal pattern formation and selection, *ACS Macro Lett.*, 2012, **1**(1), 217–221.
5 L. Li, C. M. Chan, J. X. Li, K. M. Ng, K. L. Yeung and L. T. Weng, A Direct Observation of the Formation of Nuclei and the Development of Lamellae in Polymer Spherulites, *Macromolecules*, 1999, **32**, 8240–8242.
6 L. Li, C. M. Chan, K. L. Yeung, J. X. Li, K. M. Ng and Y. Lei, Direct observation of growth of lamellae and spherulites of a semicrystalline polymer by AFM, *Macromolecules*, 2001, **34**(2), 316–325.
7 X. Wang, W. Zhou, Y. G. Lei, C. M. Chan, J. X. Li and K. M. Ng, *et al.*, The Birth of an Embryo and Development of the Founding Lamella of Spherulites As Observed by Atomic Force Microscopy, *Macromolecules*, 2002, **35**(18), 6751–6753.
8 C. M. Chan and L. Li, Direct Observation of the Growth of Lamellae and Spherulites by AFM, *Adv. Polym. Sci.*, 2005, **188**, 1–41.
9 Y. Jiang, D. D. Yan, X. Gao, C. C. Han, X. G. Jin and L. Li, *et al.*, Lamellar branching of poly(bisphenol A-*co*-decane) spherulites at different temperatures studied by high-temperature AFM, *Macromolecules*, 2003, **36**(10), 3652–3655.
10 Y. Yang, H. Tian, S. Napolitano and B. Zuo, Crystallization in thin films of polymer glasses: The role of free surfaces, solid interfaces and their competition, *Prog. Polym. Sci.*, 2023, **144**, 101725.
11 Y. Liang, M. Zheng, K. H. Park and H. S. Lee, Thickness-dependent crystal orientation in poly(trimethylene 2,6-naphthalate) films studied with GIWAXD and RA-FTIR methods, *Polymer*, 2008, **49**(7), 1961–1967.
12 J. P. Yang, Q. Liao, J. J. Zhou, X. Jiang, X. H. Wang and Y. Zhang, *et al.*, What determines the lamellar orientation on substrates?, *Macromolecules*, 2011, **44**(9), 3511–3516.
13 K. B. Shepard and R. D. Priestley, MAPLE deposition of macromolecules, *Macromol. Chem. Phys.*, 2013, **214**(8), 862–872.
14 R. D. Torres, S. L. Johnson, R. F. Haglund, J. Hwang, P. L. Burn and P. H. Holloway, Mechanisms of resonant infrared matrix-assisted pulsed laser evaporation, *Crit. Rev. Solid State Mater. Sci.*, 2011, **36**(1), 16–45.
15 H. Jeong, S. Napolitano, C. B. Arnold and R. D. Priestley, Irreversible Adsorption Controls Crystallization in Vapor-Deposited Polymer Thin Films, *J. Phys. Chem. Lett.*, 2017, **8**(1), 229–234.
16 Z. Zhang, J. Ding, B. M. Ocko, J. Lhermitte, J. Strzalka and C. H. Choi, *et al.*, Nanoconfinement and Salt Synergistically Suppress Crystallization in Polyethylene Oxide, *Macromolecules*, 2020, **53**(4), 1494–1501.

17 Y. Suzuki, H. Duran, M. Steinhart, H. J. Butt and G. Floudas, Homogeneous crystallization and local dynamics of poly(ethylene oxide) (PEO) confined to nanoporous alumina, *Soft Matter*, 2013, **9**(9), 2621–2628.
18 M. Zhang, B. H. Guo and J. Xu, A Review on Polymer Crystallization Theories, *Crystals*, 2016, **7**(1), 4.
19 S. N. Magonov, V. Elings and M. H. Whangbo, Phase imaging and stiffness in tapping-mode atomic force microscopy, *Surf. Sci.*, 1997, **375**, L385–L391.
20 A. Fang and M. Haataja, Crystallization in organic semiconductor thin films: A diffuse-interface approach, *Phys. Rev. E: Stat., Nonlinear, Soft Matter Phys.*, 2014, **89**(2), 1–9.
21 Y. Wang, C. M. Chan, K. M. Ng and N. Li, What controls the lamellar orientation at the surface of polymer films during crystallization?, *Macromolecules*, 2008, **41**(7), 2548–2553.
22 G. Zhang, X. Zhai, Z. Ma, L. Jin, P. Zheng and W. Wang, *et al.*, Morphology diagram of single-layer crystal patterns in supercooled poly(ethylene oxide) ultrathin films: Understanding macromolecular effect of crystal pattern formation and selection, *ACS Macro Lett.*, 2012, **1**(1), 217–221.